Available online at www.sciencedirect.com

SciVerse ScienceDirect

Advances in Space Research xxx (2013) xxx–xxx

ADVANCES IN SPACE RESEARCH (a COSPAR publication)

www.elsevier.com/locate/asr

Rarefied gas effects on the aerodynamics of high area-to-mass ratio spacecraft in orbit

Craig White [a,*], Camilla Colombo [a,b], Thomas J. Scanlon [a], Colin R. McInnes [a], Jason M. Reese [a]

[a] Department of Mechanical and Aerospace Engineering, University of Strathclyde, Glasgow G1 1XJ, UK
[b] Faculty of Engineering and the Environment, University of Southampton, Highfield, Southampton SO17 1BJ, UK

Received 10 July 2012; received in revised form 30 December 2012; accepted 2 January 2013

Abstract

The aerodynamic situation of a satellite-on-a-chip operating in low Earth orbit bears some resemblance to a classical Crookes radiometer. The large area-to-mass ratio characteristic of a SpaceChip means that very small surface-dependent forces produce non-negligible accelerations that can significantly alter its orbit. When the temperature of a SpaceChip changes, the drag force can be changed: if the temperature increases, the drag increases (and vice versa). Analytical expressions available in the literature that describe the change in drag coefficient with orbit altitude and SpaceChip temperature compare well with our direct simulation Monte Carlo results presented here. It is demonstrated that modifying the temperature of a SpaceChip could be used for relative orbit control of individual SpaceChips in a swarm, with a maximum change in position per orbit of 50 m being achievable at 600 km altitude.

Keywords: SpaceChip; Rarefied gas; DSMC; Position control

1. Introduction

In this paper we investigate rarefied gas effects on orbiting high area-to-mass spacecraft. Recent advances in miniaturisation enable the fabrication of such spacecraft, with sensing, computing and communication capabilities within to the dimensions of a single microchip. These are so-called "satellites-on-a-chip" or "SpaceChips" (Barnhart et al., 2007).

Miniaturisation reduces production, launch and deployment costs, hence vast numbers of 'smart dust' devices can be fabricated for use in swarm applications (Colombo and McInnes, 2012; Colombo et al., 2013). Increased launch opportunities and low manufacturing costs reduce the total mission cost. For this reason SpaceChips can accept higher risk in investigating new phenomena or exploring the harsh space environment. Their fundamental payload and power limitations mean that they are ideally suited for distributed sensor networks with separations of less than one kilometre. SpaceChips are cost-effective and mass-producible, and would most usefully carry out brief, but novel, distributed sensing missions in low-Earth orbit.

A high surface-area-to-mass ratio is typical of these miniature spacecraft. As mass scales with length as L^3, while surface area scales as L^2, the effective areal density scales as L^{-1} with diminishing spacecraft size. For high area-to-mass spacecraft, surface perturbations, such as solar radiation pressure (SRP) and atmospheric drag, are therefore no longer negligible. For example, solar radiation pressure was found to reduce the perigee of the ECHO balloon satellite by 44 km in the first 12 days of its mission (Shapiro and Jones, 1960). Rather than being counteracted, surface perturbations could instead be exploited to generate new

* Corresponding author.
E-mail addresses: craig.white@strath.ac.uk (C. White), c.colombo@soton.ac.uk (C. Colombo), tom.scanlon@strath.ac.uk (T.J. Scanlon), colin.mcinnes@strath.ac.uk (C.R. McInnes), jason.reese@strath.ac.uk (J.M. Reese).

0273-1177/$36.00 © 2013 COSPAR. Published by Elsevier Ltd. All rights reserved.
http://dx.doi.org/10.1016/j.asr.2013.01.002

families of highly perturbed non-Keplerian orbits and potentially new mission applications (Colombo and McInnes, 2010). The SpaceChip considered in this paper has dimensions of 1 cm × 1 cm × 25 μm (Atchison and Peck, 2010), and an area-to-mass ratio of 17.39 m^2/kg. Fig. 1 is an example of how the acceleration due to atmospheric drag changes with area-to-mass ratio of four different spacecraft: LAGEOS (Johnson et al., 1976), a CubeSat (Heidt et al., 2000), ECHO (Shapiro and Jones, 1960), and a SpaceChip (Atchison and Peck, 2010). For the purposes of this example, it has been assumed that each spacecraft is orbiting at 600 km, and it is clear that the acceleration due to drag is significantly more important for the higher area-to-mass ratio satellites (the ECHO balloon and a SpaceChip).

A SpaceChip is usually considered to operate isothermally (Barnhart et al., 2007; Atchison and Peck, 2010). Here we assume that this is not the case; in fact, if there is a temperature gradient across the shortest side of the SpaceChip it may experience forces akin to those generated in a Crookes radiometer (Crookes, 1875). Objects in the exosphere can have a significant temperature difference across them: the Sun-facing side can be at a significantly higher temperature than the shaded side. Although SpaceChips are thin and would reach an equilibrated temperature quickly (Barnhart et al., 2007), insulating layers and heater plates could be implemented to maintain a temperature gradient across them. Gas-molecule surface interactions are highly influenced by the surface temperature, particularly in the transition and free-molecular Knudsen number regimes. Here we will first investigate whether a temperature gradient across the SpaceChip can generate additional radiometric forces, and then we will study how the surface temperature affects the drag coefficient. Since atmospheric drag remains the most important force at the altitudes we are most interested in, it is assumed throughout this paper that the forces and accelerations due to solar radiation pressure will not be modified by any heater plates or insulating layers added. Also, the orbit perturbation due to the Earths oblateness will be neglected in this study, as it does not depend on the spacecraft parameters, hence it cannot be engineered as a means of control. This allows an investigation solely of the effects of the radiometric forces and SpaceChip temperature on the drag coefficient.

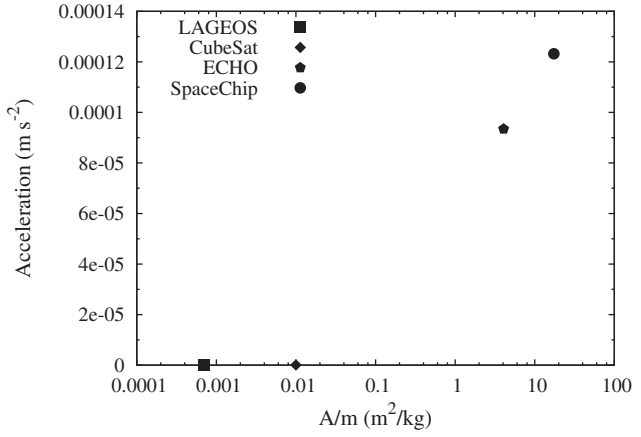

Fig. 1. Acceleration due to atmospheric drag against area-to-mass ratio A/m for several different spacecraft at 600 km altitude.

Our numerical simulations use the direct simulation Monte Carlo (DSMC) method (Bird, 1994; Scanlon et al., 2010) for rarefied gas flows, and we compare our results to various analytical expressions for the radiometric force (Gimelshein et al., 2011b) and drag coefficient (Bird, 1994; Storch, 2002), with the aim of defining the ranges of validity of these analytical expressions.

Finally, we propose that modifying the temperature could be used as a means of precision control in the position of different SpaceChips in a swarm. We also investigate the feasibility of surface temperature changes as means of attitude control by exploiting moments created by uneven surface heating.

2. Rarefied gas dynamics

Traditionally, in the modelling of gas flows, the assumption that the fluid can be considered as a continuum is valid and the usual linear constitutive relations and no-slip and no-temperature jump boundary conditions follow (Gad-el-Hak, 1999). However, when the gas is very rarefied or if the length scales involved in the problem become very small, the continuum assumption breaks down and some interesting and non-intuitive effects can emerge, e.g., velocity slip, temperature jump, and thermal creep. The Knudsen number,

$$Kn = \frac{\lambda}{L}, \tag{1}$$

is a measure of the degree of rarefaction in a gas. Here the mean free path λ is the average distance a gas molecule travels before it collides with another molecule, and L is a characteristic length scale. As the magnitude of the Knudsen number increases, the relative importance of gas rarefaction effects increases. The Knudsen number regimes and the appropriate flow models to be used in each of them can be summarised as (Gad-el-Hak, 1999):

- $Kn \to 0$: inviscid flow (Euler equations);
- $Kn \leqslant 0.001$: continuum regime (Navier–Stokes–Fourier equations);
- $0.001 \leqslant Kn \leqslant 0.1$: slip regime (Navier–Stokes–Fourier; equations with slip and jump boundary conditions);
- $0.1 \leqslant Kn \leqslant 10$: transition regime (Boltzmann equation or particle methods);
- $Kn \geqslant 10$: free-molecular regime (Boltzmann equation or particle methods).

Fig. 2 is a graphical illustration of these different Knudsen number regimes. In the SpaceChip system we

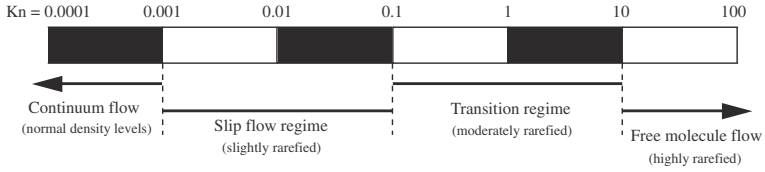

Fig. 2. Knudsen number regimes, adapted from Gad-el-Hak (1999).

investigate here, the mean free path will be very large, while the characteristic length scale is 1 cm, leading to a large Knudsen number. Therefore, our investigations are primarily within the free-molecular regime, where inter-molecular collisions are unlikely to occur, but gas molecule interactions with surfaces are still important.

In the transition and free-molecular regimes the Boltzmann equation should be solved to provide an accurate solution of the gas flow, which, for a single species monatomic gas, is:

$$\frac{\partial(nf)}{\partial t} + \xi_j \frac{\partial(nf)}{\partial x_j} + F_j \frac{\partial(nf)}{\partial \xi_j} = J(f, f^*), \tag{2}$$

where nf is the product of the number density and velocity distribution function, ξ_j and x_j are the speed and position of a molecule respectively, and F_j is an external force. This equation is difficult to solve analytically and numerically because of the non-linear form of the collision integral $J(f, f^*)$, which is

$$J(f, f^*) = \int_{-\infty}^{\infty} \int_{0}^{4\pi} n^2 \left(f^* f_1^* - f f_1\right) \xi_r \sigma_{cr} d\Omega(\xi)_1, \tag{3}$$

where the superscript * represents post-collisional properties, ξ_r is the relative velocity of the two colliding molecules, σ_{cr} is the collision cross-section, d is the molecular diameter, and Ω is the solid angle. While the Boltzmann equation needs to be used for transition regime flows, this does present a significant problem because inter-molecular collisions are still important in this regime. The free-molecular regime is less of a problem because inter-molecular collisions are unlikely and so the collision term can be ignored.

3. Radiometric forces

A rarefied gas surrounding a thin plate – such as a Crookes radiometer vane, or a SpaceChip – with a temperature difference between its two largest sides results in a force being generated that tends to move the plate in the direction from the hot to the cold side. This radiometric force is composed of three components and a recent detailed analysis of it can be found in Gimelshein et al. (2011b), Selden et al. (2009) and Gimelshein et al. (2011a). An example of radiometric forces being used for a practical purpose can be found in Ota et al. (2007) and He et al. (2009), where remote laser heating is used to heat a vane assembly in a rarefied gas environment with application as a microactuator.

It should be noted that the flow Mach numbers produced in the rarefied gas as a result of radiometric effects are typically very small. This presents problems for any particle-based numerical simulation method that has to recover macroscopic fields from a spatial and time average of individual particle properties. Such methods include DSMC and molecular dynamics (MD): the signal-to-noise ratio is very low and the number of samples required to reduce the noise is proportional to the inverse of the Mach number squared (Hadjiconstantinou et al., 2003). Fortunately, it is easier to recover fields such as forces that act on a given geometry, as these are measured from the difference in pre- and post-collision properties of the particles that interact with a surface.

4. Numerical technique

We use the direct simulation Monte Carlo method (Bird, 1994) to obtain solutions for rarefied gas flows in the transition and free molecular regimes. DSMC is a particle-based stochastic method that is valid over the full Knudsen number range. The only constraint on using DSMC is that the gas must be dilute (i.e., the mean molecular separation should be far greater than the molecular diameter), so that only binary inter-molecular collisions are likely to occur.

The DSMC method decouples the particle movements and collisions, which enables a relatively large numerical time step size to be accessed. A single DSMC particle can represent any number of real molecules, which dramatically reduces the computational expense of a simulation. Particle movements are handled ballistically according to their individual velocities and the global time step, while interactions with the boundaries and inter-particle collisions are dealt with in a stochastic manner. DSMC has emerged over the past 40 years to be the dominant numerical technique for simulating rarefied gas flows in the transition and free molecular regimes. It has been proven to provide an exact solution to the Boltzmann equation as the number of particles tends to infinity (Wagner, 1992).

The numerical mesh for a DSMC simulation performs two separate tasks and must take into account the size of the mean free path. The dimensions of a cell should be smaller than the mean free path; the usual recommendation is that the cell dimensions are less than one third of the mean free path. This is so that macroscopic gradients can be captured with sufficient resolution. It is also normal to split each cell into a set of virtual sub-cells during the collision process. Only particles within the same virtual sub-cell are considered for collision with one another, thereby increasing the physical realism of a simulation by

Please cite this article in press as: White, C., et al. Rarefied gas effects on the aerodynamics of high area-to-mass ratio spacecraft in orbit. J. Adv. Space Res. (2013), http://dx.doi.org/10.1016/j.asr.2013.01.002

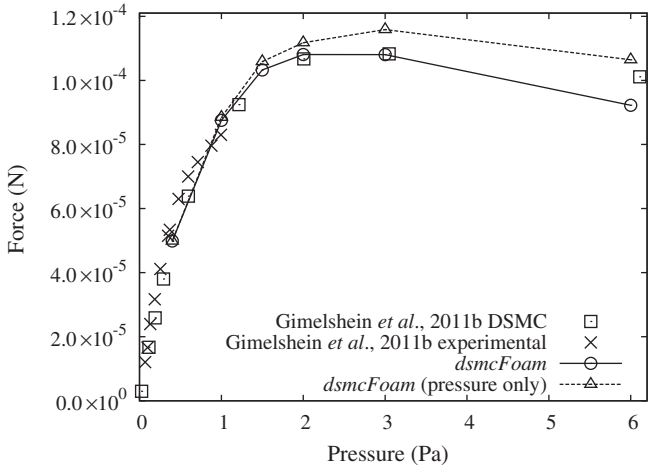

Fig. 3. Radiometric forces obtained experimentally and calculated by the SMILE code, compared with those calculated using the *dsmcFoam* code.

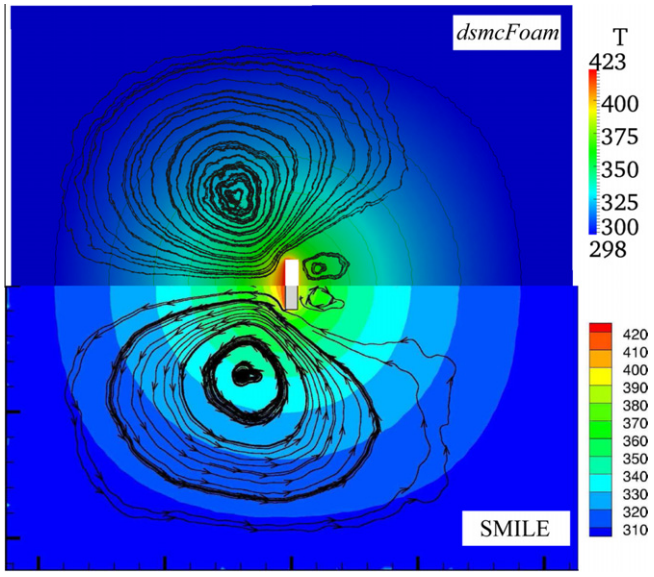

Fig. 4. Contours of temperature with velocity streamlines for argon gas at Kn = 0.12. Comparison of results from SMILE (bottom) and *dsmcFoam* (top) codes.

promoting nearest-neighbour collisions. Time step sizes must be smaller than the mean collision time (the average time a molecule takes between successive collisions), but it is also desirable that the time step is small enough that particles are likely to spend several time steps within a single cell, giving them ample opportunity to undergo a collision.

The DSMC solver used in our work is *dsmcFoam*, which is implemented within the open-source C++ fluid dynamics toolbox OpenFOAM (www.openfoam.org). We have previously rigorously verified and validated this for a range of benchmark cases (Scanlon et al., 2010; Arlemark et al., 2012). The variable hard sphere (VHS) collision model (Bird, 1983) is implemented within *dsmcFoam* and provides collision cross sections that are proportional to the relative collision energy of the particle pair being considered for collision. It has been shown to provide values of mean free path that are consistent with experimental and theoretical results. The phenomenological Larsen-Borgnakke model (Borgnakke and Larsen, 1975) is used to redistribute energy between internal particle modes and the translational modes, and the no-time-counter (NTC) scheme (Bird, 1994) is used when determining how many collision pair candidates should be selected in order to obtain the correct collision frequency rates. The validation cases considered in Scanlon et al., 2010 were typically supersonic or hypersonic DSMC cases. The flows involved with radiometric forces are however considerably different from these kinds of flows and so *dsmcFoam* is validated here against previous numerical work on radiometer vanes.

The chosen validation test case is a heated plate in a vacuum chamber, which has been investigated both experimentally and numerically (Gimelshein et al., 2011b). The gas inside the chamber is evacuated to different pressures, allowing a range of degrees of rarefaction to be tested. The plate has a constant temperature gradient across its thickness, generated by maintaining one side at 450 K and the other at 410 K. The chosen gas for simulation is helium, because it gives a larger force value than heavier gases such as argon or nitrogen. The plate dimensions are 13.12 cm × 3.81 cm × 0.95 cm and the chamber dimensions are 0.4 m × 0.4 m × 0.4 m. The chamber walls are maintained at a constant 300 K throughout and the Knudsen numbers tested range from 0.076 to 1.143 based on the VHS mean free path and the plate length of 3.81 cm.

Fig. 3 shows the values of the forces measured by *dsmcFoam* compared with those reported by Gimelshein et al., which were produced using the well known Statistical Modeling In Low density Environment (SMILE) DSMC code (Ivanov et al., 2006), and experimental results (Gimelshein et al., 2011b). Excellent agreement is found between the two independent codes, demonstrating that *dsmcFoam* is capable of capturing the flow phenomena and forces associated with radiometric applications. The *dsmcFoam* results also show that including the shear forces reduces the force compared to when only the pressure component is included.

Fig. 4 shows contours of temperature with velocity streamlines for argon as the working gas at a Knudsen number of 0.12, from both SMILE and *dsmcFoam*. Good qualitative agreement is found: the temperature contours are very similar, and both codes predict a large recirculation region on the hot side of the vane, with a smaller recirculation zone immediately behind the cold side.

5. Non-isothermal SpaceChips

In this section it is considered that the larger sides of a SpaceChip are at different temperatures – either passively (as a result of one side facing the Sun and the other being in shade with an insulating layer between the two sides), or actively controlled through a system such as a heater plate. Alternatively, electrochromic coating could be used, but

Please cite this article in press as: White, C., et al. Rarefied gas effects on the aerodynamics of high area-to-mass ratio spacecraft in orbit. J. Adv. Space Res. (2013), http://dx.doi.org/10.1016/j.asr.2013.01.002

Table 1
Atmospheric composition at different altitudes, H; n is number density, i.e., the number of molecules of the indicated species per unit volume.

H (km)	n_{O_2} (m^{-3})	n_{N_2} (m^{-3})	n_O (m^{-3})	n_{Ar} (m^{-3})	n_{He} (m^{-3})	n_H (m^{-3})
75	1.522×10^{20}	5.726×10^{20}	–	–	–	–
100	2.151×10^{18}	9.210×10^{18}	4.298×10^{17}	9.501×10^{16}	1.133×10^{14}	–
200	1.918×10^{14}	2.925×10^{15}	4.050×10^{15}	1.938×10^{12}	1.310×10^{13}	1.630×10^{11}
400	1.252×10^{11}	4.669×10^{12}	9.583×10^{13}	2.124×10^{8}	4.868×10^{12}	8.960×10^{10}
600	1.880×10^{8}	1.575×10^{10}	3.707×10^{12}	6.351×10^{4}	2.154×10^{12}	7.231×10^{10}
800	4.105×10^{5}	7.377×10^{7}	1.732×10^{11}	3.027×10^{1}	1.001×10^{12}	5.961×10^{10}
1000	1.251×10^{3}	4.626×10^{5}	9.562×10^{9}	2.188×10^{-2}	4.850×10^{11}	4.967×10^{10}
1300	4.084×10^{2}	1.510×10^{5}	3.122×10^{9}	7.143×10^{-3}	1.583×10^{11}	1.620×10^{10}

this will also alter the forces due to solar radiation pressure, which may dominate in this situation. DSMC simulations are now conducted considering a 50 K temperature difference across the thickness of the SpaceChip. While this is a very large temperature difference, the statistical nature of the numerical technique makes it prohibitively computationally expensive to simulate flows with temperature differences of 5 K or below; however, low variance DSMC methods (Radtke et al., 2011) could be implemented in *dsmcFoam* in the future to remove this restriction. Low Earth orbit altitudes from 75 km to 1300 km are considered and SpaceChip flows are simulated in two dimensions using *dsmcFoam*. Comparison is then made with analytical solutions for both the radiometric force and the drag coefficient in the free-molecular flow regimes.

The case of a SpaceChip orbiting the Earth has similarities to the heated plate in a vacuum chamber. The surrounding gas is rarefied because of the extremely low gas density in the upper reaches of the atmosphere and, as outlined above, a temperature gradient is present across the 25 μm thickness of the SpaceChip (Atchison and Peck, 2010). This differs from previous numerical work on radiometer vanes and similar geometries because the gas is not single species and indeed even changes composition as altitude changes. Table 1 shows the atmospheric composition variation with altitude, taken from the US Standard Atmosphere 1976 (NASA, 1976). The surrounding gas temperature initially decreases with altitude, but then rises to reach 1000 K by around 250 km (NASA, 1976). A thermal analysis (Atchison and Peck, 2010) of a SpaceChip geometry found that the surface temperatures of the chip would be well below the surrounding gas temperature at altitudes above 150 km.

Previous numerical work has been on vanes in stationary gases, or exposed to only very modest velocities (Cornella et al., 2010). However, the SpaceChip will be exposed to free stream velocities of approximately 7000 m/s as it orbits the Earth. It may be expected that the extremely low density wake produced behind a SpaceChip will prevent a radiometric force from being produced, but that similar rarefied gas physics should mean that the drag force acting on the SpaceChip will vary with surface temperature.

The velocity at which the SpaceChip orbits in the atmosphere is

$$U_\infty = \sqrt{\frac{\mu_{\text{Earth}}}{r_{\text{orbit}}}}, \tag{4}$$

where μ_{Earth} is the gravitational parameter of the Earth, and the orbit radius r_{orbit} is defined as $(R_{\text{Earth}} + H)$, where R_{Earth} is the radius of the Earth. The velocity U_∞ and atmospheric temperature T_∞ are given in Table 2 (the rotational velocity of the atmosphere has been neglected here).

The theoretical drag forces acting on the SpaceChip at each altitude can be calculated using the drag equation,

$$F_{\text{drag}} = \frac{1}{2} c_D \rho_\infty A U_\infty^2, \tag{5}$$

where c_D is the drag coefficient, ρ_∞ is the freestream atmospheric density, and A is the cross-sectional area exposed to the flow; c_D has initially been estimated to be 2.1 for the SpaceChip geometry. It is usual for preliminary mission analysis studies to consider a constant drag coefficient in the range 2.1 – 2.2 (Villamil et al., 1912). Table 2 contains the calculated values for the drag forces.

5.1. Stationary SpaceChips

First, we consider SpaceChips that are artificially stationary with respect to the atmosphere, in order to help distinguish radiometric force effects from atmospheric drag. All of the altitudes and gas compositions given in Tables 1 and 2 are simulated in DSMC. Fig. 5 is a schematic of the forces expected to be acting on these artificially stationary SpaceChips. The hot sides are considered to be at a constant temperature of 405 K, the cold sides are constant at 355 K and molecule-surface interactions are fully diffuse. The average temperature of 380 K is consistent with that predicted for a SpaceChip in orbit (Barnhart et al., 2007; Atchison and Peck, 2010).

Table 3 shows the information used to determine the cell sizes and time steps required to obtain reliable DSMC results. In all of our simulations, the gas is simulated as a multi-component particle mixture. The mean free path λ, mean collision time t_{mc} and most probable thermal velocity V_{mp} are taken from the US Standard Atmosphere 1976 (NASA, 1976); nEqParticles is the number of real molecules/atoms that each DSMC simulator particle represents. The parameters have been chosen so that each simulation contains the same number of DSMC particles, and that each cell in the mesh initially contains a sufficient number

Please cite this article in press as: White, C., et al. Rarefied gas effects on the aerodynamics of high area-to-mass ratio spacecraft in orbit. J. Adv. Space Res. (2013), http://dx.doi.org/10.1016/j.asr.2013.01.002

Table 2
Atmospheric temperature, SpaceChip orbit velocity and analytical drag forces at different altitudes.

H (km)	T_∞ (K) (NASA, 1976)	U_∞ (m/s)	Analytical drag force (N)
75	208.4	7859	0.23
100	195.1	7840	3.42×10^{-3}
200	854.6	7780	1.77×10^{-6}
400	995.8	7670	1.70×10^{-8}
600	995.9	7560	8.72×10^{-10}
800	1000	7450	6.82×10^{-11}
1000	1000	7350	1.71×10^{-11}
13000	1000	7205	6.32×10^{-12}

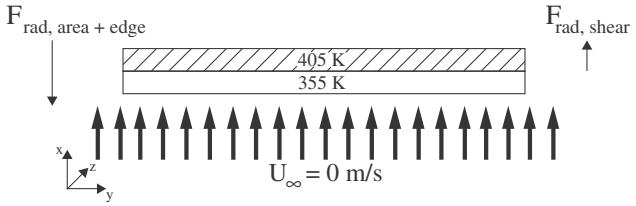

Fig. 5. Schematic of the forces acting on an artificially stationary SpaceChip: $F_{\text{rad,area+edge}}$ are the edge and area forces described in Gimelshein et al. (2011b) and $F_{\text{rad,shear}}$ is the shear force.

Table 3
DSMC simulation parameters.

H (km)	λ (m)	t_{mc} (s)	nEqParticles	V_{mp} (m/s)
75	2.3×10^{-3}	6.0×10^{-6}	1.6×10^{9}	388.7
100	1.4×10^{-1}	3.7×10^{-4}	1.1×10^{7}	381.4
200	2.4×10^{2}	0.3	6460.0	921.6
400	1.6×10^{4}	13.9	96.0	1148.5
600	2.8×10^{5}	208.3	5.0	1356.3
800	1.4×10^{6}	714.3	1.1	1954.3
1000	3.1×10^{6}	1333.3	0.5	2318.1
1300	1×10^{7}	3333.3	0.16	2500.0

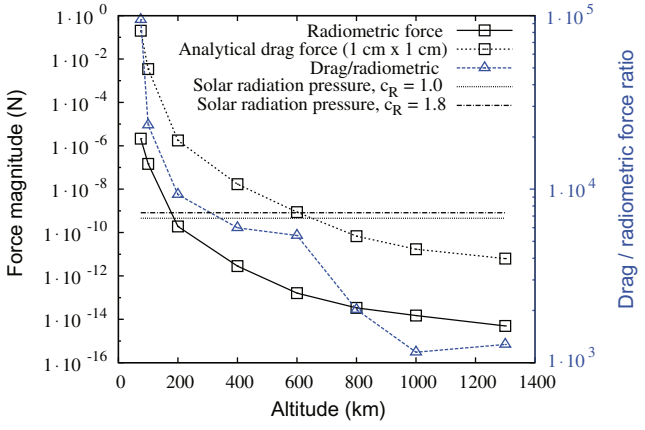

Fig. 6. Variation of radiometric forces with altitude. The theoretical drag force is shown for reference, and the ratio of the two forces has also been plotted.

of particles to meet good DSMC practice. The measured statistical error in each of the force results in the stationary SpaceChip cases with a 50 K temperature difference is approximately ±2%, which is deemed acceptable for the current work. This statistical error was calculated as the standard error in the instantaneous force measurements.

Fig. 6 shows the computed radiometric forces acting on the stationary SpaceChip at different altitudes. The solar radiation pressure for reflectivity coefficients c_R of 1.0 and 1.8 are also shown for reference, along with the analytical drag force using a drag coefficient of 2.1. The range of applicability of this drag coefficient will be tested in a later section.

Fig. 6 shows that the predicted radiometric forces are around three to four orders of magnitude smaller than the expected drag forces, with the radiometric force becoming slightly more important as the altitude increases. The measured forces are all very small, but so is the mass of the SpaceChip (around 5.75×10^{-6} kg): the acceleration due to the radiometric force at 600 km is 3.5×10^{-9} m/s^2. It is interesting to note that at this altitude the accelerations due to drag and solar radiation pressure are expected to be of roughly the same magnitude. At altitudes below 600 km, atmospheric drag is the dominant force and at higher altitudes, forces due to solar radiation pressure dominate. Therefore, any rarefied gas effects that can be taken advantage of will be most effective at altitudes of up to 600 km.

An analytical solution for the radiometric force in the free-molecular regime is given in Gimelshein et al. (2011b) as:

$$F = \frac{P}{2} A \left(\sqrt{\frac{\sigma_M T_h + (1-\sigma_M) T_\infty}{T_\infty}} - \sqrt{\frac{\sigma_M T_c + (1-\sigma_M) T_\infty}{T_\infty}} \right), \tag{6}$$

where P is the freestream pressure, σ_M is Maxwell's accommodation coefficient, and T_h and T_c are the temperature of the hot and cold side of the radiometer vane, respectively.

Table 4 compares the forces calculated using Eq. (6) with those obtained from our DSMC simulations. At 75 km altitude, the flow is clearly not free-molecular and elements of collisional flow are dominating, which Eq. (6) cannot account for. From 100 km and up, the flow can be considered close to free-molecular – demonstrated by the analytical and numerical results being in good agreement.

5.2. Orbiting SpaceChips

We now consider a SpaceChip travelling at the velocity at which it would orbit the Earth at each altitude

Table 4
Force per unit pressure values, calculated from our simulations and an independent analytical approach.

H (km)	F/P_{sim} (N/Pa)	F/P_{analy} (N/Pa)	Ratio
75	1.090×10^{-6}	4.444×10^{-6}	0.245
100	4.569×10^{-6}	4.594×10^{-6}	0.995
200	2.244×10^{-6}	2.195×10^{-6}	1.022
400	1.958×10^{-6}	2.033×10^{-6}	0.963
600	1.988×10^{-6}	2.029×10^{-6}	0.978
800	1.978×10^{-6}	2.029×10^{-6}	0.975
1000	1.981×10^{-6}	2.029×10^{-6}	0.977
1300	2.022×10^{-6}	2.029×10^{-6}	0.996

Table 5
Forces obtained from DSMC simulations on orbiting SpaceChips with the flow incident on either the hot or the cold face.

H (km)	F_{cold} (N)	F_{hot} (N)
75	2.017×10^{-1}	2.017×10^{-1}
100	3.445×10^{-3}	3.458×10^{-3}
200	1.637×10^{-6}	1.643×10^{-6}
400	1.777×10^{-8}	1.785×10^{-8}
600	7.089×10^{-10}	7.128×10^{-10}
800	7.208×10^{-11}	7.258×10^{-11}
1000	2.278×10^{-11}	2.297×10^{-11}
1300	7.175×10^{-12}	7.241×10^{-12}

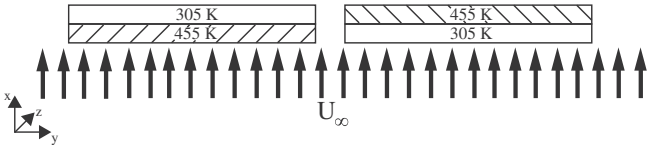

Fig. 7. Schematic of orbiting non-isothermal SpaceChip simulations. Left: flow incident on the hot face; right: flow incident on the cold face.

considered, as set out in Table 2. We consider the maximum drag configuration, i.e., when the SpaceChip lies perpendicular to the flow. The stablisation of the SpaceChip at its maximum drag configuration could be achieved by equipping the SpaceChip with a long, thin, wire antenna, although this proposal has not yet been verified. In this case, a near-vacuum wake will be produced immediately downstream of the SpaceChip. It is therefore possible that the gas flow will not experience the temperature gradient between the two faces. In order to test this, isothermal cases are also performed where the orbiting SpaceChips have a uniform temperature equal either to that of the hot face or the cold face of a non-isothermal SpaceChip.

Table 5 shows the forces computed on non-isothermal SpaceChips travelling so the gas is incident on either the hot (see Fig. 7, left side) or cold (see Fig. 7, right side) face of the SpaceChip, F_{hot} and F_{cold} respectively. The measured statistical error for these forces is around $\pm 0.015\%$, and the difference between the two forces at each altitude is comfortably outside of this statistical error range (for all altitudes above 75 km).

Table 6 compares the drag forces on the isothermal SpaceChips at 800 km with those for the non-isothermal SpaceChips at the same altitude. The temperature for each non-isothermal case is the temperature of the side of the SpaceChip that the gas flow is incident on, while in the isothermal cases the whole SpaceChip is at the stated temperature. The forces are very similar and fall within the measured statistical error of $\pm 0.015\%$. Therefore, as expected, we can say that there is no radiometric contribution to the overall force acting on a SpaceChip in orbit, because the region immediately downstream of the SpaceChip is effectively a vacuum. The only force that needs to be accounted for is a standard aerodynamic pressure drag force for this maximum drag configuration.

Despite there not being any substantive radiometric force contribution, it is still evident that when the surface temperature of the SpaceChip changes, the drag force changes: an increase in temperature increases the drag. Although this is not a radiometric force, it can be understood through the same reasoning considered for the free-molecular pressure force contribution to the overall radiometric force as described in Gimelshein et al. (2011b). At altitudes of 100 km and above, the gaseous flow is in the free-molecular regime, so inter-molecular collisions are not significant. The pre-interaction momentum remains unchanged as the surface temperature changes. When molecules collide with the surface they are reflected, but do not deflect oncoming molecules as would happen in the transition and continuum regimes. This means that the molecule flux hitting the surface is unaffected by the surface temperature, and so the pressure at the surface which results in the drag force is simply related to the difference in momentum of molecules before and after they interact with the surface.

As it has also been demonstrated that it is the temperature of the side on which the gas is incident that is important, and not the temperature difference between the two sides, we consider all SpaceChips to be isothermal in the remainder of this section. The results from Table 5 can still be used for this purpose, as the results in Table 6 demonstrate. The difference in the drag forces on a hot (405 K) and on a cold (355 K) SpaceChip is defined as

$$F_{\Delta} = \left| \frac{|F_{hot}| - |F_{cold}|}{2} \right|. \quad (7)$$

Table 6
Comparison of forces in the isothermal and non-isothermal SpaceChip cases at 800 km.

Temperature (K)	355		405	
	Isothermal	Non-isothermal	Isothermal	Non-isothermal
Force (N)	7.2075×10^{-11}	7.2078×10^{-11}	7.2563×10^{-11}	7.2578×10^{-11}

Please cite this article in press as: White, C., et al. Rarefied gas effects on the aerodynamics of high area-to-mass ratio spacecraft in orbit. J. Adv. Space Res. (2013), http://dx.doi.org/10.1016/j.asr.2013.01.002

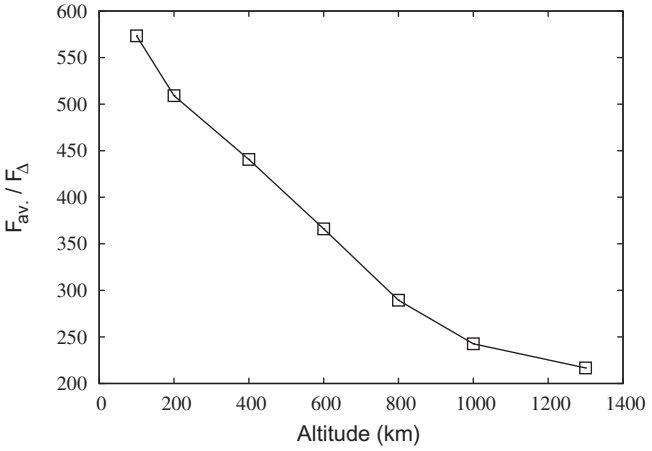

Fig. 8. Variation of $F_{av.}/F_{\Delta}$ with altitude.

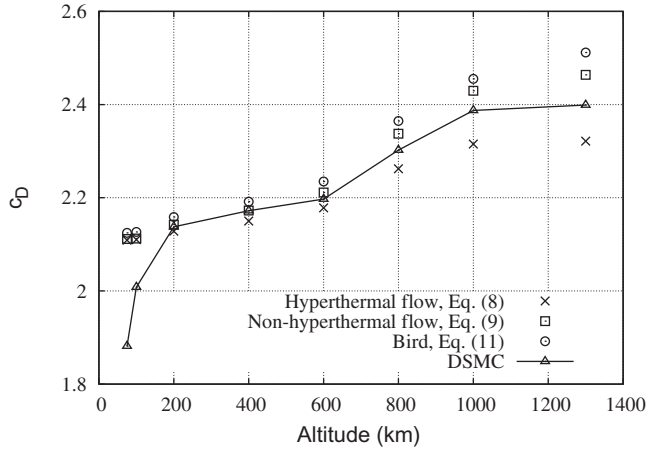

Fig. 9. Variation of c_D with altitude, calculated using different analytical and DSMC solutions, for a SpaceChip temperature of 405 K.

Then the ratio of the force acting on an isothermal SpaceChip at the average temperature $F_{av.}$ to F_{Δ} can be used to evaluate how much of an effect changing the spacecraft's temperature has on the drag force.

A set of DSMC simulations at the average temperature of 380 K were performed. Fig. 8 shows a plot of this ratio $F_{av.}/F_{\Delta}$ varying with altitude, with F_{hot} and F_{cold} being found for temperatures of 405 K and 355 K respectively.

Clearly F_{Δ} increases (relative to the drag force at the average temperature $F_{av.}$) with altitude. Since the drag force can be altered by changing the surface temperature (provided no other parameters are altered), it is concluded that the drag coefficient is changing with the spacecraft's temperature.

6. Drag coefficient

There are several analytical solutions available for calculating the drag coefficient of a flat plate in a free-molecular flow. Two different expressions are given in Storch (2002): one for hyperthermal flow and one for non-hyperthermal flow, where a hyperthermal flow is defined as one in which the thermal component of the gas molecular velocities is negligible compared to the macroscopic velocity, i.e., $U_{\infty} \gg V_{mp}$. It is not always certain that the flow in the current work can be considered hyperthermal (e.g., at 1000 km, $V_{mp}/U_{\infty} = 0.315$) and so both forms of the analytical expression are considered here. The hyperthermal and non-hyperthermal equations are given as

$$c_{D_{\text{hyperthermal}}} = 2\left[\sigma_M + \sigma_M \frac{V_w}{U_{\infty}} \sin(\alpha) + (2 - 2\sigma_M)\sin^2(\alpha)\right] \sin(\alpha), \tag{8}$$

and

$$\begin{aligned} c_{D_{\text{non-hyperthermal}}} = {} & 2\sigma_M \frac{V_w}{U_{\infty}} \sin^2(\alpha) + \frac{2}{\sqrt{\pi} s} \\ & \left[(2 - \sigma_M)\sin^2(\alpha) + \sigma \cos^2(\alpha)\right] \exp(-s^2 \sin^2(\alpha)) \\ & + 2\left[(2 - \sigma_M)\left(\sin^2(\alpha) + \frac{1}{2s^2}\right) + \sigma_M \cos^2(\alpha)\right] \\ & \times \sin(\alpha)\text{erf}(s \sin(\alpha)), \end{aligned} \tag{9}$$

respectively, where

$$V_w = \sqrt{\frac{\pi k T_w}{2m}}, \tag{10}$$

s is the molecular speed ratio, k is the Boltzmann constant, T_w is the SpaceChip temperature, m is the molecular mass, and σ_M is Maxwell's accommodation coefficient.

Note that as s tends to ∞, Eq. (9) reduces to Eq. (8). A further analytical expression from Bird, 1994 is given as

$$\begin{aligned} c_{D_{\text{Bird}}} = {} & 2\frac{\{1 - \varepsilon\cos(2\alpha)\}}{\sqrt{\pi} s} \exp\left(-s^2 \sin^2(\alpha)\right) \\ & + \frac{\sin(\alpha)}{s^2}\left[1 + 2s^2 + \varepsilon\left\{1 - 2s^2\cos(2\alpha)\right\}\right]\text{erf}(s \\ & \times \sin(\alpha)) + \frac{(1 - \varepsilon)}{s}\sqrt{\pi}\sin^2(\alpha)\left(\frac{T_w}{T_{\infty}}\right)^{\frac{1}{2}}, \end{aligned} \tag{11}$$

where $\varepsilon = 1 - \sigma_M$.

In Fig. 9, results from Eqs. (8)–(11) are compared to the drag coefficients obtained from our DSMC simulations for flow incident on an isothermal SpaceChip with a surface temperature of 405 K.

The three different analytical expressions and our DSMC solution follow the general trend of drag coefficient increasing with altitude, with the DSMC solutions within 5% of the analytical results. The DSMC results do not match the analytical solutions at 75 km and 100 km: in Section 5.1 it was established that the flow is not free-molecular at 75 km, so this is expected. However, at 100 km the flow is free-molecular for the case of a stationary SpaceChip, but this does not appear to be the case for an orbiting SpaceChip. The large velocity leads to an increased density at the forward stagnation point and this increase in density is large enough to reduce the local mean free path, making

Table 7
Drag coefficients from Eq. (11) for different surface accommodation coefficients.

H (km)	c_D		
	$\sigma_M = 1$	$\sigma_M = 0.8$	$\sigma_M = 0.5$
75	2.117	2.494	3.061
100	2.119	2.496	3.062
200	2.149	2.525	3.089
400	2.181	2.554	3.113
600	2.222	2.591	3.143
800	2.346	2.704	3.242
1000	2.433	2.786	3.316
1300	2.487	2.838	3.364

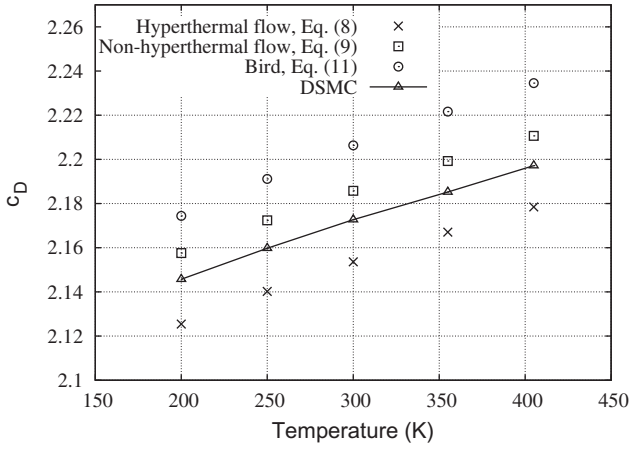

Fig. 10. Variation of c_D with different SpaceChip temperatures, at an altitude of 600 km.

inter-molecular collisions important in the stagnation region, despite them being negligible in the freestream.

All of our work has so far considered fully diffuse surfaces, but the drag coefficient is expected to be highly sensitive to different values of the accommodation coefficient. For example, Table 7 shows the drag coefficients obtained using Eq. (11) for a surface temperature of 355 K, but with different accommodation coefficients. A vacuum environment has a 'cleaning' effect on surfaces and results in a surface that is less than fully accommodating (Bird, 1994). A real surface, for which $\sigma_M < 1$, may have a significantly greater drag coefficient than a perfectly diffuse surface. On the other hand, atomic oxygen adsorption on the surface of a satellite may cause the accommodation coefficient to remain close to unity (Moe and Moe, 2005).

In the case of a specular reflection, the normal component of the incident velocity simply changes sign. For the SpaceChips considered here, the magnitude of the reflected normal component from a diffuse reflection will (on average) be smaller because the surface temperature T_w is lower than the free-stream temperature T_∞. A reduced accommodation coefficient means an increased number of specular reflections, and hence an increase in the drag coefficient. The SpaceChip will not equilibrate to the free stream gas temperature as the power flux from the incident gas molecules is negligible compared to that from the radiation from the sun, and so does not greatly affect the radiative energy balance when calculating the SpaceChip temperature.

Determination of accommodation coefficients are often made experimentally and must take into account the surface material, surface roughness and gas composition. For example, in Graur et al., 2009 the accommodation coefficients for silicon micro-channels conveying argon and nitrogen gas are determined by comparing experimental results for the mass flow rates with analytical solutions for Poiseuille flow. Molecular dynamics simulations can also be used to determine accommodation coefficients, but it is important to use accurate molecule-molecule and molecule-surface interaction potentials, and this data is not always readily available (Daun et al., 2011; Kovalev and Yakunchikov, 2010).

The magnitude of the changes in the drag force that can be obtained by increasing or decreasing the surface temperature are relatively small, producing a difference $\mathcal{O}(10^{-14})$ N for a 25 K temperature increase or decrease. The difference in drag force will be much smaller for smaller temperature changes, but the statistical nature (and low signal-to-noise characteristics) of DSMC makes simulating such small temperature differences impractical. However, a small change in drag force could be used to advantage in missions involving swarms of SpaceChips. If a means of controlling the temperature of individual SpaceChips can be implemented, e.g., through an integral heater plate, it will be possible to use this change of temperature as a control method for changing the relative positions of individual SpaceChips within a swarm. The magnitude of the force would be predictable and repeatable and the fact that it is extremely small would allow for precise position control of individual SpaceChips. This close control application would be most applicable at orbit altitudes between 200 km and 600 km, where modifying the drag coefficient can have a decisive effect on the overall force acting on a SpaceChip.

Fig. 10 shows the predicted drag coefficients from our DSMC simulations alongside the analytical solutions at 600 km, as the temperature increases from around the minimum to the maximum predicted temperatures for a SpaceChip (Barnhart et al., 2007; Atchison and Peck, 2010). The DSMC results match the analytical expressions well, particularly the non-hyperthermal flow solution of Eq. (9). It is clear that it is possible to exert a small degree of control over the drag coefficient at this altitude through modifying the surface temperature.

6.1. Position control

Assuming a SpaceChip of dimensions of 1 cm × 1 cm × 25 μm with a density equal to that of silicon (2300 kg m^{-3}), the total control acceleration available between temperatures of 200 K and 405 K is 2.9×10^{-6} m s^{-2}. For a circular orbit at 600 km, having a period of 5820 s, the inter-spacecraft change in velocity Δv per orbit

is 0.017 m s^{-1} and the inter-spacecraft displacement Δs per orbit is therefore 50 m. This means that it is possible to alter the position of a single SpaceChip with respect to another one by up to 50 m in a single orbit by modifying the surface temperature to increase or decrease the drag coefficient. Smaller temperature differences will lead to smaller Δs, e.g., changing surface temperature from 300 K to 355 K gives a control acceleration of 7.05×10^{-7} m s^{-2} and Δs per orbit is reduced to 12 m. This demonstrates that very small temperature differences could be used to produce useful values of Δv and Δs for performing position control.

A drag coefficient of 2.1 is commonly used when performing preliminary SpaceChip mission analysis but, as we have shown, the drag coefficient (considering fully diffuse surfaces) can vary from around 1.9–2.5 as altitude and SpaceChip temperature increases. When more realistic accommodation coefficients of less than 1 are considered, the drag coefficient values are even greater.

Until now, it has been considered that the SpaceChips will remain perfectly perpendicular to the flow, and that they are at exactly the same altitude. In reality, this is not sustainable (e.g., due to the effect of variable wind direction on drag); therefore, a disturbance analysis is carried out. To study the effect of aerodynamic disturbances on inter-spacecraft displacement per orbit, it is first considered that one SpaceChip remains at the maximum drag configuration, while a second one can have angles of attack up to $\pm 20°$ from the maximum drag configuration. We then consider that two SpaceChips with the same attitude can be at different altitudes. Note that, if we assume that the change in temperature does not affect the reflectivity coefficient, the characteristic acceleration due to solar radiation pressure can be considered constant in low Earth orbit at 602 and 598 km. It has been demonstrated (Atchison and Peck, 2011), at altitudes of around 600 km and a length scale of 1 cm, that accelerations due to drag are more significant than those due to solar radiation pressure. In addition, it has been shown that the accelerations due to magnetism, in the form of Lorentz accelerations, are significantly less important than atmospheric drag accelerations at this altitude.

The distance between two SpaceChips in a distributed sensor network is not likely to be greater than 1 km, as discussed in Section 1, so an analysis of an altitude separation of up to 4 km is considered sufficient here. The drag coefficients for the analysis have been calculated using Eq. (11).

In order to study the effect of the angle of attack α on the inter-spacecraft displacement of two SpaceChips at different temperatures and an altitude of 600 km, the parameter Δc_D is introduced:

$$\Delta c_D = \left(c_{D_{200\,\mathrm{K},\alpha=90}} - c_{D_{405\,\mathrm{K},\alpha}}\right), \tag{12}$$

or

$$\Delta c_D = \left(c_{D_{405\,\mathrm{K},\alpha=90}} - c_{D_{200\,\mathrm{K},\alpha}}\right), \tag{13}$$

when the SpaceChip at 200 K is at constant angle of attack or the one at 405 K is at constant angle of attack, respectively; $c_{D_{200\mathrm{K},\alpha=90}}$ and $c_{D_{405\mathrm{K},\alpha=90}}$ are the drag coefficients when the temperature is 200 K or 405 K, and the angle of attack is constant at 90°, and $c_{D_{200\mathrm{K},\alpha}}$ and $c_{D_{405\mathrm{K},\alpha}}$ are the drag coefficients for SpaceChips at temperatures of 200 K and 405 K respectively, at angle of attack α.

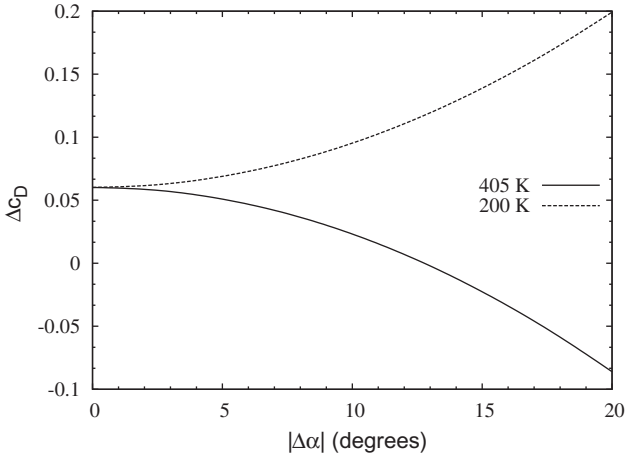

Fig. 11. Variation of Δc_D with change in angle of attack $|\Delta\alpha|$ at 600 km for SpaceChips at 200 K and 405 K. The legend indicates which SpaceChip is having its angle of attack altered.

Fig. 11 shows the variation of Δc_D for different angles of attack, where $|\Delta\alpha|$ is the difference in angle of attack between the two SpaceChips. When the SpaceChip at 405 K has its angle of attack varied with respect to the one at 200 K, it is clear that the change in drag coefficient decreases, hence a smaller control acceleration is available in this situation. Until the situation where the 405 K SpaceChip has an angle of attack of 77° or 103° ($\Delta\alpha = 13°$) it is still possible to create a positive control acceleration. For example, using Eq. (11), when both have $\alpha = 90°$ the inter-spacecraft displacement in one orbit is 59 m, but when the 405 K SpaceChip has an angle of attack of 11° this is reduced to 14 m. On the other hand, it is found that varying the angle of attack of the SpaceChip at 200 K always increases the control acceleration available. When the 200 K SpaceChip has an angle of attack of 11°, the inter-spacecraft displacement in a single orbit is increased to 100 m.

If two SpaceChips are not at the same altitude, they will experience slightly different forces due to the different atmospheric densities and orbital velocities. Here, we consider an altitude of 600 ± 2 km. If the 405 K SpaceChip is at 602 km and the 200 K one is at 598 km, the control acceleration available is 1.58×10^{-6} m s^{-2}, which is around half that available when both are at an altitude of 600 km. If the 200 K SpaceChip is at 602 km and the 405 K one is at 598 km, the control acceleration is around double that when both are at 600 km: 5.25×10^{-6} m s^{-2}.

For both attitude and altitude differences, it is clear that the aerodynamic disturbances can enhance or restrict the level of position control available to a SpaceChip operator. Position control is still achievable in all but one of our studied disturbances – it is not found when the SpaceChip

Please cite this article in press as: White, C., et al. Rarefied gas effects on the aerodynamics of high area-to-mass ratio spacecraft in orbit. J. Adv. Space Res. (2013), http://dx.doi.org/10.1016/j.asr.2013.01.002

has a relative angle of attack $\Delta\alpha$ of 13° with respect to the 200 K one which is at the maximum drag coefficient.

In addition to altitude and attitude differences between individual SpaceChips, the atmospheric conditions themselves are dependent on a number of factors that the US Standard Atmosphere (NASA, 1976) model considered in the current work does not account for. Solar activity is one such factor, and it has been found that periods of exceptional solar activity increase the local density and alter the atmospheric composition at orbital altitudes where the drag force is still dominant (Willis et al., 2005; Berger et al., 1998).

6.2. Attitude control

Previously it was considered that the SpaceChip temperature was uniform. However, if its temperature could be modified non-uniformly it should be possible to create a moment around the centre of mass. This moment could be used to change the attitude of individual SpaceChips. A similar strategy for attitude control was proposed for the IKAROS solar sail mission, although based in that case on changing the reflectivity coefficient: a solar sail was designed with some variable reflectance elements loaded near the tips of the sail membrane. By changing the reflectivity coefficient, control of the spin direction was achieved (Kawaguchi et al., 2009). In a similar way here, a change of drag coefficient can be exploited to control the attitude of a SpaceChip (or even a solar sail in the atmosphere) without the use of a propellant.

In order to test if it is indeed possible to create a moment that could be used to control the attitude of individual SpaceChips at an altitude of interest (identified as 600 km), a SpaceChip with a non-uniform temperature is considered: one half of the SpaceChip is maintained at 355 K, and the other half at 405 K, see Fig. 12.

We performed a two-dimensional DSMC simulation of this geometry at 600 km, and measured the moments around the centre of mass of the SpaceChip at steady-state. With respect to Fig. 12, the moments considered here will be around the z-axis. A moment of -1.78×10^{-12} N m is produced by the hot half of the SpaceChip, while the cold side produces a moment of 1.77×10^{-12} N m. The overall moment around the centre of mass is -1×10^{-14} N m, so the SpaceChip will rotate slowly in an anti-clockwise direction. The moment of inertia of the SpaceChip geometry considered here is 4.79×10^{-11} kg m^2; therefore an angular acceleration of 1.2×10^{-2} deg s^{-2} (2.1×10^{-4} rad s^{-2}) is induced.

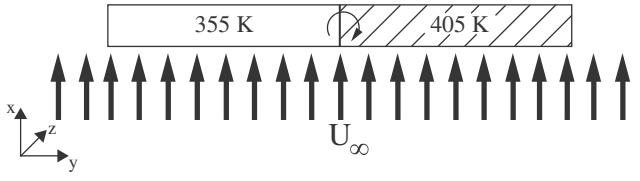

Fig. 12. Schematic of SpaceChip non-uniform temperature geometry considered for attitude control.

Similar to position control, disturbance torques can be important in any spacecraft and here we perform an analysis of these disturbances. Larson and Wertz, 1999 states the most important disturbance torques are gravity gradient, solar radiation, magnetic field, and aerodynamic force. The gravity gradient torque T_g is calculated as (Larson and Wertz, 1999):

$$T_g = \frac{3\mu_{\text{Earth}}}{2r_{\text{orbit}}}|I_x - I_z|\sin(2\theta), \tag{14}$$

where I_x and I_z are the mass moments of inertia around the x and z axes of Fig. 12, respectively, and θ is the angular deviation from the local horizontal. The maximum gravity gradient disturbance for the 20° angle of attack disturbance at 600 km considered is considerably less than the control torque available; 2.88×10^{-17} N m, and so is not important.

The magnetic field torque is given by $T_m = DB$, where D is the residual dipole of the SpaceChip, and B is the Earth's local magnetic field. We assume best and worst case residual magnetic dipoles of 2.5×10^{-10} A m^2 and 2.5×10^{-9} A m^2, respectively (Atchison and Peck, 2011). The worst case magnetic field at the poles for an altitude of 600 km is 4.69×10^{-5} T, reducing to half of this in the best case at the equator. This gives a worst case magnetic torque of 1.17×10^{-13} N m and a best case of 5.86×10^{-15} N m. The magnitude of the temperature-based control torque is slightly greater than the best case magnetic disturbance, indicating that a small amount of attitude control could be exercised around the equator for this example. Nearer the poles the magnetic disturbance torque is greater than the control torque we calculated would be available.

The aerodynamic torque is:

$$T_a = F_{\text{drag}}(c_{pa} - c_g), \tag{15}$$

where c_{pa} is the centre of pressure, and c_g is the centre of gravity. The centre of pressure position with changing angle of attack has been estimated using Avanzini's law (40):

$$c_{pa} = L(0.2 + 0.3\sin\alpha), \tag{16}$$

where L is the SpaceChip length. With this estimate for the position of c_{pa}, and assuming that the centre of gravity is at the geometrical centre of the SpaceChip, the magnitude of the aerodynamic disturbance torque is found to be greater than the control torque of 1×10^{-14} N m once the angle of attack is ±5° from the maximum drag configuration. At our 20° maximum disturbance, the aerodynamic torque is much larger than the control torque; 1.2×10^{-13} N m.

The solar radiation pressure disturbance torque is proportional to the difference in position between the centre of gravity and the centre of solar pressure. Since we are considering that the solar radiation pressure forces and accelerations remain constant as the temperature changes, our centre of solar pressure will not move, and we assume it is at the same position as the centre of gravity; hence,

there is no disturbance torque due to solar radiation pressure in our current analysis.

For the large temperature difference considered in this example, the available angular slew is only 5°; smaller temperature differences would create smaller control torques and so it is found that non-uniform temperature control is not a practical control method for SpaceChips in low Earth orbit.

7. Conclusions

An analysis of rarefied gas effects on the aerodynamics of orbiting non-isothermal SpaceChips has been performed using the DSMC computational method, and the results have been compared where possible with analytical solutions for free-molecular flow.

A non-isothermal SpaceChip that is stationary with respect to the atmosphere experiences a free-molecular radiometric force at altitudes of 100 km and above. When an orbiting velocity is incorporated, no evidence of radiometric forces was found because no molecules are able to interact with the trailing surface of the SpaceChip as the wake behind it is effectively a vacuum.

Free-molecular analytical solutions for the drag coefficient are in good agreement with our numerical results for altitudes of 200 km and above. It was found that the drag coefficient can vary from 1.9 to 2.5 for a SpaceChip temperature of 405 K as the altitude increases from 75 km to 1300 km. Small changes in drag coefficient with changing surface temperature at the same altitude have also been found. For example, at 600 km, increasing the SpaceChip temperature from 200 K to 405 K resulted in the drag coefficient changing from 2.15 to 2.2. Reducing the surface accommodation coefficient in order to consider a more realistic surface that has been 'cleaned' by exposure to a vacuum environment led to further increases in the drag coefficient: as high as 3.36 for an accommodation coefficient of 0.5 at 1300 km. However, there is evidence to suggest that atomic oxygen adsorption on the surface of a satellite will keep the accommodation coefficient close to unity.

At altitudes below 600 km, atmospheric drag forces have been found to dominate in comparison to forces due to solar radiation pressure. At altitudes of up to 600 km advantage could be taken of changing the drag force to create a decisive change in the overall force acting on a SpaceChip. Although the change in force would clearly be very small, the high area-to-mass ratio of a SpaceChip means that the accelerations due to this change in force are relatively large. This could be advantageous for precision position control of individual SpaceChips within a swarm. At 600 km, it has been found that the position of a single SpaceChip can be altered by up to 50 m in a single orbit by modifying its surface temperature between the highest and lowest predicted temperatures for a SpaceChip in orbit. An analysis of disturbances indicated that a degree of control was available for two SpaceChips with slightly different attitudes and altitudes than they may have in reality.

A natural extension to the opportunity for position control would be that of attitude control by modifying the temperature of a SpaceChip non-uniformly. It has been demonstrated that torques could be produced in this way, but a disturbance analysis has indicated that aerodynamic disturbances will prevent attitude control slews of greater than 5° at 600 km. In addition, the magnetic field disturbance torque makes any attitude control unfeasible for the SpaceChip we have considered, unless it is orbiting near the equator. Small, more realistic, temperature differences would also greatly decrease the available control torques.

Acknowledgements

Craig White was funded by a scholarship from the James Weir Foundation. Camilla Colombo was funded by the European Research Council, as part of project VISIONSPACE (227571). Our calculations were performed on the 1100 core HPC Facility of the Faculty of Engineering at the University of Strathclyde. The authors would like to thank Dr Ricky Martin for technical support on the HPC.

References

Arlemark, E., Markelov, G., Nedea, S. Rebuilding of Rothes nozzle measurements with OpenFOAM software. JPCS 362, 012040, 2012.

Atchison, J.A., Peck, M.A. A passive, sun-pointing, millimeter-scale solar sail. Acta Astronaut. 67 (1–2), 108–121, 2010.

Atchison, J.A., Peck, M.A. Length scaling in spacecraft dynamics. J. Guid. Contr. Dyn. 34 (1), 231–245, 2011.

Barnhart, D.J., Vladimirova, T., Sweeting, M.N. Very-small-satellite design for distributed space missions. J. Spacecraft Rockets 44 (6), 1294–1306, 2007.

Berger, C., Biancale, R., Ill, M., Barlier, F. Improvement of the empirical thermospheric model DTM: DTM94 – a comparative review of various temporal variations and prospects in space geodesy applications. J. Geodesy 72, 161–178, 1998.

Bird, G.A. Definition of mean free path for real gases. Phys. Fluids 26 (11), 3222–3223, 1983.

Bird, G.A. Molecular Gas Dynamics and the Direct Simulation of Gas Flows, Oxford Science Publications. Oxford University Press Inc, New York, 1994.

Borgnakke, C., Larsen, P.S. Statistical collision model for Monte Carlo simulation of polyatomic gas mixture. J. Comput. Phys. 18 (4), 405–420, 1975.

Colombo, C., Lücking, C., McInnes, C.R. Orbit evolution, maintenance and disposal of SpaceChip swarms through electro-chromic control. Acta Astronaut. 82 (1), 25–37, 2013.

Colombo, C., McInnes, C.R. Orbital dynamics of smart dust devices with solar radiation pressure and drag. J. Guid. Contr. Dyn. 34 (6), 1613–1631, 2010.

Colombo, C., McInnes, C.R. Orbit design for future SpaceChip swarm missions in a planetary atmosphere. Acta Astronaut. 75, 25–41, 2012.

Cornella, B., Ketsdever, A.D., Gimelshein, N.E., Gimelshein, S.F. Analysis of multi-vane radiometers in high-altitude propulsion. In: 10th AIAA/ASME Joint Thermophysics and Heat Transfer Conference, 2010.

Crookes, W. On attraction and repulsion resulting from radiation – Part II. Proc. R. Soc. Lond. 23, 373, 1875.

Daun, K.J., Karttunen, M., Titantah, J.T. Molecular dynamics simulation of thermal accommodation coefficients for laser-induced incandescence sizing of nickel nanoparticles, in: Proceedings of the ASME

2011 International Mechanical Engineering Congress & Exposition, 2011.

Gad-el-Hak, M. The fluid mechanics of microdevices – the Freeman Scholar lecture. J. Fluids Eng. 121 (1), 533, 1999.

Gimelshein, N.E., Gimelshein, S.F., Ketsdever, A.D., Selden, N.P. Shear force in radiometric flows. AIP Conf. Proc. 1333 (1), 661–666, 2011a.

Gimelshein, S.F., Gimelshein, N.E., Ketsdever, A.D., Selden, N.P. Analysis and applications of radiometric forces in rarefied gas flows. AIP Conf. Proc. 1333 (1), 693–700, 2011b.

Graur, I.A., Perrier, P., Ghozlani, W., Méolans, J.G. Measurements of tangential momentum accommodation coefficient for various gases in plane microchannel. Phys. Fluids 21 (10), 102004, 2009.

Hadjiconstantinou, N.G., Garcia, A.L., Bazant, M.Z., He, G. Statistical error in particle simulations of hydrodynamic phenomena. J. Comput. Phys. 187 (1), 274–297, 2003.

He, Y., Stefanov, S.K., Ota, M. The Monte Carlo simulation of a model microactuator driven by rarefied gas thermal effects, in: Rarefied Gas Dynamics: 26th International, Symposium, 2009.

Heidt, H., Puig-Suari, J., Moore, A.S., Nakasuka, S., Twiggs, R.J. CubeSat: A new generation of picosatellite for education and industry low-cost space experimentation, in: Proceedings of the 14th Annual AIAA/USU Conference on Small Satellites, 2000.

Ivanov, M.S., Kashkovsky, A.V., Gimelshein, S.F., Markelov, G.N., Alexeenko, A.A., Bondar, Y.A., Zhukova, G.A., Nikiforov, S.B., Vashenkov, P.V. 2006. SMILE system for 2 D/3 D DSMC computations, in: Proceedings of the 25th International Symposium on Rarefied Gas, Dynamics, 539–544.

Johnson, C.W., Lundquist, C.A., Zurasky J.L. The LAGEOS satellite. Anaheim International Astronautical Federation Congress. Vol. 1, 1976.

Kawaguchi, J., Mimasu, Y., Mori, O., Funase, R., Yamamoto, T., Tsuda, Y. IKAROS – ready for lift-off as the worlds first solar sail demonstration in interplanetary space, in: 60th International Astronautical Congress, 2009.

Kovalev, V.L., Yakunchikov, A.N. Accommodation coefficients for molecular hydrogen on a graphite surface. Fluid D 45 (6), 975–981, 2010.

Larson, W.J., Wertz, J.R. (Eds.). Space Mission Analysis and Design. Kluwer Academic Publishers (Dordrecht), The Netherlands, 1999.

Moe, K., Moe, M.M. Gas surface interactions and satellite drag coefficients. Planet. Space Sci. 53, 793–801, 2005.

NASA. NASA-TM-X-74335, US Standard Atmosphere. Tech. rep., 1976.

Ota, M., He, Y., Stefanov, S.K. Monte Carlo simulation of rotation of a laser opto-microactuator, in: Rarefied Gas Dynamics: 25th International, Symposium, 2007.

Radtke, G.A., Hadjiconstantinou, N.G., Wagner, W. Low-noise Monte Carlo simulation of the variable hard sphere gas. Phys. Fluids 23 (3), 030606, 2011.

Scanlon, T.J., Roohi, E., White, C., Darbandi, M., Reese, J.M. An open source, parallel DSMC code for rarefied gas flows in arbitrary geometries. Comput. Fluids 39 (10), 2078–2089, 2010.

Selden, N.P., Ngalande, C., Gimelshein, N.E., Gimelshein, S.F., Ketsdever, A.D. Origins of radiometric forces on a circular vane with a temperature gradient. J. Fluid Mech. 634, 419–431, 2009.

Shapiro, I.I., Jones, H.M. Perturbations of the orbit of the ECHO balloon. Science 132 (3438), 1484–1486, 1960.

Storch, J.A. Aerodynamic disturbances on spacecraft in free-molecular flow. Tech. rep, DTIC Document, 2002.

Vallado, D.A. Fundamentals of Astrodynamics and Applications. Space Technology Library (New York, 2007).

Villamil, R.D., Avanzini, G. Laws of Planes Moving at an Angle in Air and Water. Forgotten Books, The Laws of Avanzini, 1912.

Wagner, W.A. convergence proof for Birds direct simulation Monte Carlo method for the Boltzmann equation. J. Stat. Phys. 66, 1011–1044, 1992.

Willis, P., Deleflie, F., Barlier, F., Bar-Sever, Y.E., Romans, L.J. Effects of thermosphere total density perturbations on LEO orbits during severe geomagnetic conditions (Oct–Nov 2003) using DORIS and SLR data. Adv. Space Res. 36 (3), 522–533, 2005.

Please cite this article in press as: White, C., et al. Rarefied gas effects on the aerodynamics of high area-to-mass ratio spacecraft in orbit. J. Adv. Space Res. (2013), http://dx.doi.org/10.1016/j.asr.2013.01.002